Anharmonic atomic vibrations in the relaxor ferroelectric Pb(Mg_{1/3}Nb_{2/3})O_{3} under pressure

Takamitsu Yamanaka, Muhtar Ahart, Yuki Nakamoto, Zuo-Guang Ye, Stephen A. Gramsch, Ho-kwang Mao, and Russell J. Hemley

Phys. Rev. B **86**, 174108 — Published 12 November 2012

DOI: 10.1103/PhysRevB.86.174108

Anharmonic atomic vibrations in the relaxor ferroelectric $Pb(Mg_{1/3}Nb_{2/3})O_3$ under pressure

Takamitsu Yamanaka[1], Muhtar Ahart[1], Yuki Nakamoto[2], Zuo-Guang Ye[3], Ho-kwang Mao[1], and Russell J. Hemley[1]

[1] *Geophysical Laboratory, Carnegie Institution of Washington*
Washington DC 20015, USA
[2] *Center for Quantum Science and Technology Under Extreme Conditions, Osaka University*
Osaka, Japan
[3]*Department of Chemistry and 4D LABS, Simon Fraser University*
Burnaby, BC, V5A 1S6, Canada
E-mail: tyamanaka@ciw.edu

Abstract

Structural analyses of the relaxor ferroelectric material $Pb(Mg_{1/3}Nb_{2/3})O_3$ (PMN) with single-crystal x-ray diffraction under pressure in a diamond anvil cell indicate static atomic displacement and chemical disorder. Difference Fourier analysis within the framework of a harmonic oscillator model for the atomic vibrations reveals residual electron density on both the Pb and Nb (Mg) sites. Pb atoms in the A site of the ABO_3 perovskite structure exhibit a greater displacement than the Nb(Mg) atoms in the B-site, despite the fact that Pb is a much heavier atom. The displacement is interpreted in terms of an anharmonic statistical atomic motion. At pressures above 2.5 GPa the displacement disappears, consistent with previous observations. The difference Fourier maps reveal no residual electron densities greater than 1 e/Å^3 at any atomic position, and these are appear to be induced by the violation of local electrical neutrality arising from both Mg^{2+} and Nb^{5+} ions located at the octahedral site. Similar electron densities are observed at all experimental pressures and in refinements based on both harmonic and anharmonic models. The anharmonic parameters taken into account are the higher-order tensors of atomic elastic motion. At high pressure, where the relaxor transforms to a paraelectric phase, the residual electron densities disappear.

Introduction

Lead-based relaxor ferroelectrics with the perovskite structure exhibit a strong frequency-dispersive dielectric permittivity with broad temperature dependence, superior piezoelectric response, and other peculiar properties [1-3]. In particular, the dielectric properties peak in a region of the phase diagram (pressure-temperature-composition) where the dielectric constant shows frequency dispersion and has a maximum with decreasing temperature. Burns et al. [2] first observed that the temperature dependence of the dielectric permittivity deviates from Curie-Weiss behavior in relaxor ferroelectrics at a specific temperature (now referred to as the Burn's temperature T_d), and suggested that the presence of polar clusters would give rise to such a deviation in the dielectric constant. In addition, their high permittivity and high piezoelectric constants make them suitable for applications in devices for sonar or medical imaging [1]. While extensive theoretical [3-7] and experimental studies [1-3, 7-12] have advanced the fundamental understanding of relaxor behavior, their properties are still poorly understood. The difficulties stem from the complexity of these materials, which have a high degree of compositional, structural and polar disorder.

It is generally admitted that the peculiar physical properties of relaxor ferroelectrics, such as diffuse phase transitions and a dielectric relaxation, are related to an intrinsic nanoscaled local structure, called polar nanoregions (PNRs) [2]. The existence of PNR clusters within average crystal structures has also been confirmed experimentally [8] but no insight has been obtained regarding their dynamical properties. Recently, first-principles based molecular dynamics simulations [6] showed that, if in addition to the regular ferroelectric effects of polar distortions and homogeneous strain, a coupling to a random field that originated from the chemically disordered regions (CDRs) was included, then one could obtain such ordered and disordered regions in polarization. It was observed that the polarization was large in the chemically ordered regions (CORs), and almost close to zero in the CDRs, suggesting that the PNRs could be chemically ordered regions. Further studies based on the same MD model [7] revealed that the diffuse scattering, another feature of the relaxors, could be attributed to strong correlations between the displacement of the Pb ion within the PNR clusters, and such correlations between Pb ions prefer a particular orientation within the crystal structure. A number of studies have addressed the phenomenon of diffuse scattering [13].

There have been several studies of the high-pressure behavior of relaxor ferroelectrics, such as $Pb(Mg_{1/3}Nb_{2/3})O_3$ (PMN) and related materials. Although PMN never enters a ferroelectric state even down to 4 K at ambient pressure, high-pressure Raman studies of relaxor PMN reveal peak

splitting (at 4.5 GPa) from a broader band centered at 270 cm^{-1} suggesting a displacement transition to a high-pressure phase [9]. In addition, recent high-pressure Brillouin scattering of PMN [14] showed an elastic anomaly near 4.5 GPa, consistent with the previous Raman studies. High-pressure x-ray diffuse scattering from PMN reveals a butterfly-shaped pattern that decreases under pressure and gradually disappears [10]. More generally, high-pressure dielectric measurements on compositionally disordered ABO_3 oxides indicate that the pressure-induced ferroelectric-to-relaxor crossover is a common phenomenon and can be explained by a decrease in the correlation length between dipole moments [11].

One of the major challenges in the analysis and understanding of relaxors is experimental access to such local properties with respect to the average structure, which is often a difficult task. In particular, the orientation of local displacements of the A-site or B-site cations is needed to understand correlations between dipole moment and other phenomena. Single crystal x-ray diffraction combined with the maximum entropy method has proven to be one of the rare techniques available for a direct observation of the characteristic local structure in materials [15,16]. Here we present an investigation of the prototype perovskite relaxor PMN using high-pressure single crystal x-ray diffraction from a synchrotron source. The polarization or dipole moment (vector), and the second-rank tensors such as dielectric susceptibility, strain tensors or stress tensors are used to describe the ferroelectric properties [17, 18]. These tensors definite orientation within a crystal and they must conform to the crystal symmetry. Anisotropy in the dynamical phenomena arises from the elasticity of the crystal, which can be interpreted by forth-rank tensors. Although the thermal vibration of atoms in a crystal is not perfectly harmonic, as is the ellipsoidal vibration represented by the second order thermal parameter, a harmonic oscillation model is a good approximation in most cases. Anharmonicity and disorder in simple and complex perovskites have been investigated using high energy synchrotron radiation and hot neutron diffraction [19]. $SrTiO_3$ and $BaTiO_3$ are quasi-harmonic systems whereas $KNbO_3$ shows weak anharmonicity and $PbTiO_3$ and the relaxor perovskites $PbSc_{1/2}Nb_{1/2}O_3$ display strong anharmonic features. The diffuse streak found for the relaxor PMN is considered due to the correlation between anisotropy of atomic displacements, thus the anisotropic anharmonic thermal vibration must be taken into account.

The purpose of the present work is to show that the atomic displacements in relaxors, particularly of the Pb ion, have a strong orientation anisotropy, and this anisotropy strongly contributes to the diffuse scattering and other properties of relaxor ferroelectrics.

Experimental

Structure refinements using x-ray single-crystal diffraction intensities from PMN under pressure were performed in order to clarify the static atomic displacement. The main focus of the analysis is the temperature factor (Debye-Waller factor) in the refinement, which is related both to atomic displacement due to thermal vibrations of the atoms and statistical positional disorder.

A PMN crystal was contained in a cramp-type diamond anvil high-pressure cell (DAC) with a large opening angle, which allowed diffraction up to $2\theta = 80^{\circ}$. The specifications of this type of DAC have been described previously [17]. A methanol-ethanol-water mixture was used as the pressure-transmitting medium, as this has proven to provide hydrostatic conditions in the DAC up to 12 GPa. Single-crystal diffraction intensity measurements on PMN at pressures of 1.4, 2.5, 3.4, 5.9 and 7.3 GPa were performed with a four-circle diffractometer and scintillation counter at BL-10A at the Photon Factory (PF), Tsukuba [20,21]. The diffractometer measures the four angles, ω, 2θ, ϕ and χ, for each reflection. A scintillation counter was used to measure the diffraction intensities, since it is capable of more precise measurements and determination of the orientation matrix than an area detector. A precise orientation matrix (UB matrix) and unit cell parameters are determined by least-squares refinement using the peak positions of more than 20 reflections, which permit the equivalent peaks to be located. An unambiguous determination of the space group can be determined from the extinction rules and reflection conditions. Three-dimensional peak profiles and the diffraction intensity of each reflection are observed. It is worth noting that diffraction intensities from a single crystal under high pressure can be more accurately measured than from a powder diffraction sample, because reflections are separately detected, even under any deviatoric stress existing in the DAC. Intensity measurements at ambient pressure were made using an 18 kW rotating-anode laboratory x-ray source (Mo$K\alpha$ radiation).

Conditions for the single crystal diffraction experiments at various pressures are summarized in Table 1. The number of observed reflections and the number of crystallographically independent reflections used in the least-squares refinements are listed in Table 2, along with refinement statistics, atomic positions, and temperature factors calculated for the harmonic and anharmonic models. Diffraction intensities were obtained from the average values of the crystallographically equivalent reflections.

Harmonic and anharmonic oscillator temperature factor and their implication

PMN has a cubic perovskite structure with space group $Pm\bar{3}m$. All atoms are located on special positions; hence there are no variable positional parameters. Consequently, only temperature factors

were investigated as a function of pressure at room temperature. First the conventional structure refinements have been carried out with the anisotropic second-order temperature factor by the full matrix least-squares program RADY [22].

The overall temperature factor, B_D, (Debye-Waller factor) is given by

$$B_D = \langle \exp(i\mathbf{q}\cdot\mathbf{u}) \rangle^2,$$

where **u** is the displacement of a scattering center, and <...> denotes either thermal or time averaging. Assuming harmonicity of the scattering centers, the Boltzmann distribution implies that **q·u** is normally distributed. Least squares structure analysis is conducted by iterative fit of atomic positions and position variability factor (temperature factor) to an electron density map.

$$B_D = 8\pi^2(\langle u_d^2 \rangle + \langle u_s^2 \rangle),$$

where $\langle u_d^2 \rangle$ is the dynamic variability in atomic location due to the temperature dependent vibration and $\langle u_s^2 \rangle$ is the static variability due to the unresolved occupancy, which is a function of the altered electron density (polarization effects) and crystal disorder.

The meaning of B_{eq} can be derived from $B_{eq} = \frac{4}{3}\left\{\sum_i \sum_j B_{ij} a_i a_j\right\}$, where a_1, a_2, a_3 are lattice constants *a, b, c,* respectively. Mean square displacement $\langle u^2 \rangle$ is defined by $\langle u^2 \rangle = U_{iso} = \frac{B_{iso}}{8\pi}$.

The structure factor is calculated by

$$F_{cal}(h) = K\sum_j a_j f_j(h) \sum T_{js}(h) \exp\left\{2\pi i(hx_{js} + ky_{js} + lz_{js})\right\} \qquad (1)$$

where K is a scale factor. a_j represents a multiplicity of reflection *hkl* defined by crystallographic symmetry. $T(h)$ is a temperature factor contributing to diffraction intensity of *hkl* and f_j indicates the atomic scattering factor of atom *j*. Fully ionized atomic scattering factors f_j were taken from *International Tables for X-ray Crystallography, Vol. IV* (1974) [23]. Anomalous dispersion parameters of $\Delta f'$ and $\Delta f''$ were taken into account in the atomic scattering factor using $f = f_o + \Delta f' + i\Delta f''$. The least-squares refinement is carried out by minimization of difference between the amplitudes of $|F_{obs}(h)|$ and $|F_{cal}(h)|$:

$$\Delta = \sum_h w(h)\left\{|F_{obs}(h)| - |F_{cal}(h)|\right\}^2 \qquad (2)$$

where $w(h)$ is a weight parameter systematically given to *hkl* reflection. The present study was

initiated by refining the temperature factor in the harmonic approximation, and all terms higher than second order were ignored.

The equivalent temperature factor B_{eq} of each atom, which expresses the isotropic spherical components of atomic vibration, is calculated from the anisotropic factors of the second rank parameters β_{ij} (= $2\pi^2\Sigma a_i^* a_j^* U_{ij}$). The temperature factor $T(h)$ is derived from β_{ij}:

$$T(h) = \beta_{11}{}^2 + \beta_{22}{}^2 + \beta_{33}{}^2 + 2(\beta_{12}\beta_{13} + \beta_{13}\beta_{23} + \beta_{23}\beta_{12}) \qquad (3)$$

Reliability parameters R (= $w\Sigma||F_{obs}| - |F_{cal}||/\Sigma|F_{obs}|$) for the least-squares refinements are shown in Table 2. (w represents a systematic weight.) The five variable parameters based on the harmonic oscillator model that are taken into account in the refinement are β_{11} (=β_{22}=β_{33}) for Pb and Nb(Mg), β_{11} (=β_{22}) and β_{33} for oxygen, and the isotropic extinction parameter G_{iso}. The converged structure parameters at each pressure are presented in Table 2. At low pressures, the R-values are somewhat larger than at high pressures when the harmonic model is used to calculate the temperature factors.

Atomic displacement parameters (ADPs) are used to describe the weakening of Bragg intensities *via* the anharmonic (static or thermal) Debye-Waller factor B_D and its real-space counterpart, the generalized atomic probability density function (pdf) [24]. Among various approaches to the anharmonic refinement, a multimodal distribution in pdf based on a Gram-Charlier series expansion was adopted. The temperature factor $T(h)$ is derived from the following expansion:

$$T(h) = \exp\left(\frac{(2\pi i)^2}{2!}\sum_p\sum_q B h_p h_q + \frac{(2\pi i)^3}{3!}\sum_p\sum_q\sum_r C h_p h_q h_r + \frac{(2\pi i)^4}{4!}\sum_p\sum_q\sum_r\sum_s D h_p h_q h_r h_s + \ldots\ldots\right), \qquad (4)$$

where B, C and D are the second-, third- and fourth-order coefficients of the Gram-Charlier series expansion and represent the anharmonic coefficients. There are six coefficients (β_{ij}) belonging to B and fifteen tensors δ_{ijkl} belonging to D among a total of 81 coefficients. All coefficients belonging to the third order C terms are invalid, as they are incompatible with the space group symmetry of the perovskite structure. With respect to space group $Pm\bar{3}m$, the site symmetry for the A- and B-sites is $m\bar{3}m$ and that of the oxygen site is 4/*mmm*. The constraints on the coefficients are presented in Table 2, in which independent variable coefficients and their covariants are listed.

Discussion

The x-ray diffuse scattering and dielectric properties of PMN relaxor ferroelectrics are related to an intrinsic nanoscaled local structure, the polar nanoregions [2, 10]. It is difficult to directly observe such local structure experimentally. In the present study, higher rank tensors were introduced to constrain the atomic displacement due to thermal vibrations of the atoms We found a hydrostatic compression of the unit cell for experimental pressures up to 7.3 GPa, without any structural transition, as shown in Fig. 1. The bulk modulus of PMN was calculated using a new derivation of the third order Birch-Murnaghan (BM) equation of state [25], resulting in K_o=106.9(2) GPa, K_o'=8.4(1) and K_o''=-0.261. These data show that PMN is considerably softer in comparison with ordinary oxide-perovskites. A large value of K_o' may be induced by PNRs and CDRs in the relaxor. The value for K_o' obtained from the BM calculation is often larger than the second-order value (K_o' = 4) than 4, but it is important to note that the BM equation is based on a thermodynamic derivation calculation and does not include the effects associated with from the grain size or grain boundary conditions that may exist in a real sample.

Diffuse streaks found along the <110> direction in the (100) reciprocal lattice plane can be interpreted with respect to the correlations between the displacements of the Pb ion within the PNR clusters [7]. One may assume that the chemical disorder between Nb and Mg in the B site would produce a larger temperature factor than that in the A site, because heavy atoms such as Pb generally show a small temperature factor. In the present data, however, the time and space average of dynamical phenomena or microdomain disorder in the PMN bulk structure is observed. Deformation of the electron density is found mainly around the Pb atom in the difference Fourier maps at lower pressures. Such a deformation allows Pb to be displaced along particular directions and that gives the orientation of correlations between Pb ions. In addition, Pb atom displays the largest temperature factor (B_{eq}) among the constituent atoms at low pressure. The displacement of Pb atoms in the A site is more noticeable than Nb(Mg) atoms in the B site, but these deformations disappear at higher pressures. The residual electron density around the B sites is not remarkable.

Difference Fourier is calculated by

$$\left\{\left|F_{obs}(hkl)\right|-\left|F_{cal}(hkl)\right|\right\}$$

The residual electron density is expressed in terms of the difference Fourier:

$$\Delta\rho(x,y,z)=\frac{1}{V}\sum_h\sum_k\sum_l\left\{\left|F_{obs}(hkl)\right|-\left|F_{cal}(hkl)\right|\right\}\exp\left\{-2\pi i(hx+ky+lz)\right\} \tag{5}$$

Difference Fourier maps based on the harmonic and anharmonic oscillator model based on data collected at 0, 1.4, 3.4 and 7.3 GPa are shown in Figs. 2 and 3. These maps show projections on

(100) in the plane of the Pb and Nb(Mg) atomic positions, respectively, and illustrate the deformation of the electron density. Residual electron densities of larger than 1 e/Å^3 are recognized at 0.7 Å apart from the Pb position at ambient pressure, which shows statistical positional disorder. At every pressure, R-factors for least-squares refinements are dramatically improved by applying the anharmonic coefficients up to fourth order (δ_{ijkl}) in comparison with the harmonic model, which only includes coefficients up to the second rank (β_{ij}). The anisotropic anharmonic coefficients are presented in Table 2. The residual electron densities shown in the difference Fourier maps can be interpreted in terms of the atomic positional disorder in the PMN sample. Diffuse streaks found along the <110> direction in the reciprocal lattice on (001) [10] can be explained by the deformation of electron density mainly around the Pb atom found in the difference Fourier maps. These deformations disappear at 3.4 GPa as PMN becomes paraelectric. These results are consistent with first-principles MD simulations [7]. Heights of the positive and negative peaks decrease in magnitude with increasing pressure and the peak positions are displaced from the centers of the atoms. These particular features observed in the difference Fourier maps may be interpreted in two ways: one is static displacement (lattice average) and the other is dynamical disorder (time average) of the atoms in the crystal structure. The mode of the pressure dependence of the residual electron densities suggests that the former is more likely and they will be ascribed to the anharmonic contribution of the atomic displacement. It is unnecessary to consider localization of bonding electrons, lone-pair electrons or aspherical distributions of excited d electrons in the present case.

The three-dimensional difference Fourier map at ambient pressure shown in Fig. 4 presents the residual electron densities around the oxygen atoms. Large electron densities between two oxygen atoms are found at all pressures in the refinements, with both the harmonic and anharmonic models. These electron densities are at no specific atomic positions and it is therefore proposed that they are representative of a violation of the local neutrality due to Mg^{2+} and Nb^{5+} located at the octahedral site, with local chemical disorder producing this residual electron density. The positions of these particular electron densities are at the electric potential minimum in the structure as shown in Figs. 2 and 3. The residual densities around atoms thus disappear at high pressure, most likely because the domain disorder or atomic displacement is homogenized or disappears above 2.5 GPa, but the chemical disorder still remains at higher pressures region.

Dielectric constant measurements were performed at various pressures up to 4 GPa and under variable frequencies from 0 to 10 kHz. The relaxor ferroelectric characteristics of PMN are diminished at extremely low pressure, and it reveals paraelectric character below 2 GPa. These measurements are also quite consistent with the present x-ray diffraction study.

Conclusion

PMN has the cubic perovskite structure with space group $Pm\bar{3}m$, and with PbO_{12} ($m\bar{3}m$) and $Nb(Mg)O_6$ ($m\bar{3}m$) polyhedra. Single crystal structure analyses of PMN at high pressures up to 7.3 GPa show that the Pb atom has the largest temperature factor, indicating the largest atomic displacement. Difference Fourier maps of the projection on (001) at z = 0.0 and z = 0.5 based on the harmonic model reveal large residual electron densities around Pb and Nb(Mg), atoms respectively. These maps indicate obviously high densities around the Pb at ambient conditions and 1.4 GPa. A non-spherical electron distribution around the Pb atom is confirmed by an anharmonic model of the atomic displacement, which results from thermal vibrations. The positive peaks appear along <100> around the Pb sites, while the residual electron density around the Nb(Mg) sites is not remarkable.

These positive and negative peaks become less intense with increasing pressure in the harmonic model and disappear from the centers of the atoms at pressures higher than 3.4 GPa. The difference Fourier maps may be interpreted by static displacement (lattice average) and dynamical disorder (time average) of the atoms. The pressure dependence of the residual electron densities suggests that the former is more possible and they will be ascribed to the anharmonic contribution to the atomic displacement. Refinements of single crystal data from the present experiments introduce a statistical approach to the analysis of atomic displacements in consideration of the forth-order tensors describing the elastic properties of PMN.

Acknowledgments

We are very much indebted to Dr. S. Gramsch of Carnegie Institution of Washington for his great efforts to the internal review. We would like to express our great thanks to Prof. T. Suzuki and Dr. T. Tanaka of the Institute of Scientific and Industrial Research at Osaka University Japan for their help in the x-ray diffraction measurements and also to Dr. M. Sakata of Center for Quantum Science and Technology Under Extreme Conditions, Osaka University for his sample preparation. This work was sponsored by the Carnegie/DOE Alliance Center (CDAC, DE-FC03-03 NA00144). Support from DOE-BES (DE-FG02-06ER46280) and EFree, an Energy Frontier Research Center funded by the U.S. Department of Energy (DOE), Office of Science, Office of Basic Energy Sciences (BES) under Grant No. DESC0001057 is also acknowledged.

References:

1. S.E. Park and T.R. Shrout, J. Appl. Phys. 82, 1804 (1997)
2. G. Burns and F.H. Dacol, Solid State Commun. 48, 853 (1983).
3. D. Viehland, S.J. Jang, L.E. Cross, and M. Wuttig, J. Appl. Phys. 68, 2916 (1990).
4. R. Pirc and R. Blinc, Phys. Rev. B 60, 13470 (1999).
5. H. Fu and R.E. Cohen, Nature 403, 281 (2000).
6. B. P. Burton, E. Cockayne, and U.V. Waghmare, Phys. Rev. B 72, 064113 (2005).
7. P. Ganesh, E. Cockayne, M. Ahart, R.E. Cohen, B. Burton, R.J. Hemley, Y. Ren, W. Yang and Z.-G. Ye, Phys. Rev. B 81, 144102 (2010).
8. H.B. Krause, J.M. Cowley, and J. Wheately, Acta Cryst. A35, 1015 (1979).
9. J. Kreisel, B. Dkhil, P. Bouvier, and J.-M. Kiat, Phys. Rev B65, 172101 (2002).
10. B. Chaabane, J. Kreisel, B. Dkhil, P. Bouvier, and M. Mezouar, Phys. Rev. Lett. 90, 257601 (2003).
11. G.A. Samara, Phys. Rev B71, 224108 (2005).
12. M. Ahart, R.E. Cohen, V. Struzhkin, E. Gregoryanz, D. Rytz, S.A. Prosandeev, H.K. Mao, and R.J. Hemley, Phys. Rev. B71, 144102 (2005).
13. P. Bonneau, et al., J. Solid State Chem. 91, 350 (1991); S.N. Gvasaliya, Europhys. Lett. 63, 303 (2003); G.Y. Xu, G. Shirane, J.R.D. Copley, P.M. Gehring, Phys. Rev. B69, 064112, (2004); B. Dkhil, J.M. Kiat, G. Calvarin, G. Baldinozzi, S.B. Vakhrushev, E. Suard, Phys. Rev. B65, 024104 (2001) ; G-M, Rotaru, et al., J. Phys. Condensed Matter 20, 104235 (2008)
14. M. Ahart, M. Somayazulu, Z.G. Ye, R.E. Cohen, H.K. Mao, and R.J. Hemley, Phys. Rev. B79, 132103 (2009).
15. T. Yamanaka, T. Okada, and Y. Nakamoto, Phys. Rev. B80, 094108 (2009).
16. T. Yamanaka, T. Mine, S. Asogawa, and Y. Nakamoto, Phys. Rev. B80, 134120 (2009)
17. M. E. Lines and A. M. Glass, *Principles and Applications of Ferroelectrics and Related Materials*, Clarendon Press, Oxford, (1977).
18. J.F. Nye, *Physical Properties of Crystals*, Clarendon Press, Oxford, (1976).
19. J.M. Kiat, G. Baldinozzi, M. Dunlop, C. Malibert, B. Dkhil, C. Menoret, O. Masson and M.T. Fernandez-Diaz, J. Phys. Condensed Matter 12, 8411 (2000)
20. T. Yamanaka, J. Synchrotron Rad. 12, 566 (2005)
21. T. Yamanaka, T. Fukuda, T. Hattori, H. Sumiya, Rev Sci Instrum. 72,1458 (2001)
22. S. Sasaki and K. Tsukimura, J. Phys. Soc. Jpn. 56, 4 (1987).

23. T. D. Hahn, *International Tables for Crystallography*, (D. Reidel Publishing Co, Boston, 1983).

24. W. Kuhs, Acta Cryst. A48, 80 (1992)

25. K. K.M. Lee, B. O'Neilla, W. R. Paneroa, S.-H. Shima, L. R. Benedettib, R. Jeanloza, Earth Planet. Sci. Lett. 223, 381 (2004).

Figure Captions

Figure 1. Unit cell volume of PMN as a function of pressure.
Error bars on the data points are smaller than the symbol size. Unit cell volume data from the powder diffraction experiments reported by Chaabane et al.[10] are also presented.

Figure 2. Difference Fourier maps of the projection on (001) for refinements based on the harmonic and anharmonic oscillator models. The residual electron density around the Pb atom is shown with a contour interval of 0.02 e/ $Å^3$ in the section of z = 0.0, x = -0.5 to 0.5, y = -0.5 to 0.5.

Figure 3. Difference Fourier maps of the projection on (001) for refinements based on the harmonic and anharmonic oscillator models. The residual electron density around the Nb(Mg) atom is shown with a contour interval of 0.02 e/ $Å^3$ in the section of z = 0.5, x = 0.0 to 1.0, y = 0.0 to 1.0.

Figure 4. Three-dimensional difference Fourier map of PMN at 1 atm for the harmonic oscillator model with a contour interval of 0.02 e/ $Å^3$. The residual electron density distribution is shown in this map.

Table 1. Experimental Conditions for Single Crystal Diffraction Measurements at High Pressure

PF station	BL-10A
Diffractometer	Four circle
Detector	Scintillation counter
Monochromator	Si(111)
Wavelength	0.6995 ~ 0.7002 Å
Collimator	100 μm
Receiving slit	1°
Driving mode	phi fixed
2 theta (max)	80°
Sample	
size	40 x 40 μm^2
thickness	20 μm
Diamond anvil	brilliant cut
culet size	300 μm
table plane	2000 μm
Gasket	stainless steel
thickness	200 μm
preindented	80 μm
sample chamber	200 μm
Backing plate	beryllium disk
Pressure medium	Methanol + ethanol + water 16:4:1
Orientation matrix	25 reflections

Table 2

Structure analysis of $Pb(Nb_{2/3}Mg_{1/3})O_3$ relaxor

Pressure (GPa)		0.0001	1.4	2.5	3.4	5.9	7.3
Source		18kW	PF	PF	PF	PF	PF
Wave length		0.7093	0.6996	0.6995	0.7000	0.7002	0.7002
No. obs		2089	381	318	450	412	390
No. used		66	40	37	37	37	37
Lattice const.		4.0448	4.0288	4.0177	4.0069	3.9832	3.9732
Cell volume		66.175	65.392	64.853	64.332	63.197	62.732
		Harmonic oscillator model					
R(F) (%)		4.73	4.60	4.92	4.55	4.14	3.79
wR(F)(%)		5.47	4.92	4.65	4.56	4.14	3.87
R(F2)(%)		5.95	5.04	5.35	4.06	7.02	4.87
wR(F2)(5)		5.14	5.08	4.63	3.54	7.17	4.19
Nb(Mg)	B(Eq)	1.79(27)	1,47(17)	1.81(18)	1.46(16)	1.18(15)	1.11(13)
Pb	B(Eq)	2.99(19)	3.59(18)	3.15(15)	3.13(14)	2.32(11)	2.22(10)
O	B(Eq)	2.30(66)	2.37(12)	2.73(9)	2.25(85)	1.82(93)	2.37(94)
Nb(Mg)	$\beta_{11}=\beta_{22}=\beta_{33}$	0.027(13)	0.022(7)	0.029(8)	0.022(7)	0.019(7)	0.017(6)
Pb	$\beta_{11}=\beta_{22}=\beta_{33}$	0.039(9)	0.055(8)	0.049(7)	0.048((6)	0.037(5)	0.035(5)
O	$\beta_{11}=\beta_{22}$	0.036(30)	0.049(03)	0.052(33)	0.037(23)	0.037(62)	0.033(48)
	β_{33}	0.034(25)	0.029(12)	0.025(18)	0.030(16)	0.032(33)	0.029(27)
		Anharmonic oscillator model					
Pressure (GPa)		0.0001	1.4	2.5	3.4	5.9	7.32
R(F)		2.84	3.32	3.60	2.64	3.21	3.28
wR(F)		2.87	3.10	3.22	2.47	3.34	3.26

$R(F^2)$	3.67	2.88	4.33	3.29	4.84	4.51
$wR(F^2)$	3.25	2.05	3.69	2.67	4.75	4.11
Nb(Mg) B(Eq)	1.53(26)	0.47(16)	1.06(27)	0.78(17)	0.35(26)	0.99(38)
Pb B(Eq)	3.68(12)	3.12(18)	2.30(16)	2.46(25)	1.53(21)	2.12(35)
O B(Eq)	2.62(1.15)	2.36(14)	2.10(.20)	2.02(32)	1.76(80)	2.14(73)
Nb(Mg)						
$b_{11}=b_{22}=b_{33}$	0.023(11)	0.007(6)	0.017(13)	0.012(16)	0.009(10)	0.016(18)
$d_{1111}=d_{2222}=d_{3333}$ (10^{-5})	0.964	-0.495	-0.292	-0.527	-0.627	-0.051
$d_{1122}=d_{1133}=d_{2233}$ (10^{-5})	1.387	-0.169	-0.281	-0.318	-0.181	-0.433
Pb						
$b_{11}=b_{22}=b_{33}$	0.056(5)	0.048(8)	0.036(7)	0.038(18)	0.019(6)	0.034(16)
$d_{1111}=d_{2222}=d_{3333}$ (10^{-5})	0.759	-0.187	-0.621	-0.763	-0.619	-0.080
$d_{1122}=d_{1133}=d_{2233}$ (10^{-5})	2.609	-0.508	-1.258	-0.999	-0.881	-0.260
O						
$b_{11}=b_{22}$	0.011(10)	0.034(07)	0.011(23)	0.020(37)	0.017(10)	0.035(23)
b_{33}	0.098(43)	0.029(99)	0.077(34)	0.038(87)	0.053(49)	0.032(24)
$d_{1111}=d_{2222}$ (10^{-5})	0.268	1.555	0.619	0.453	2.833	2.548
d_{3333} (10^{-5})	-6.826	-1.479	-3.104	-0.948	0.958	-3.005
$d_{1122}=d_{1133}$ (10^{-5})	-0.563	-0.444	-0.721	-1.653	-0.815	-0.914
d_{2233} (10^{-5})	-0.765	-0.728	-0.765	-0.199	-0.099	-0.720

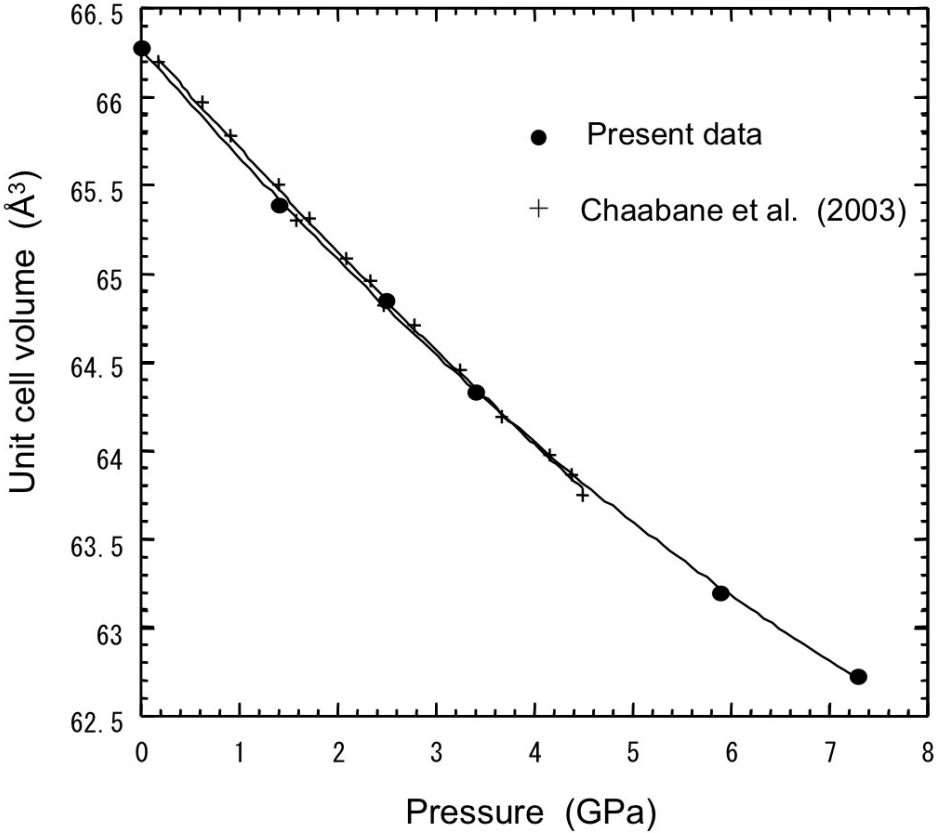
66.5
66
65.5
65
64.5
64
63.5
63
62.5
Unit cell volume (Å3)
0
1
2
3
4
5
6
7
8
Pressure (GPa)
Present data
Chaabane et al. (2003)

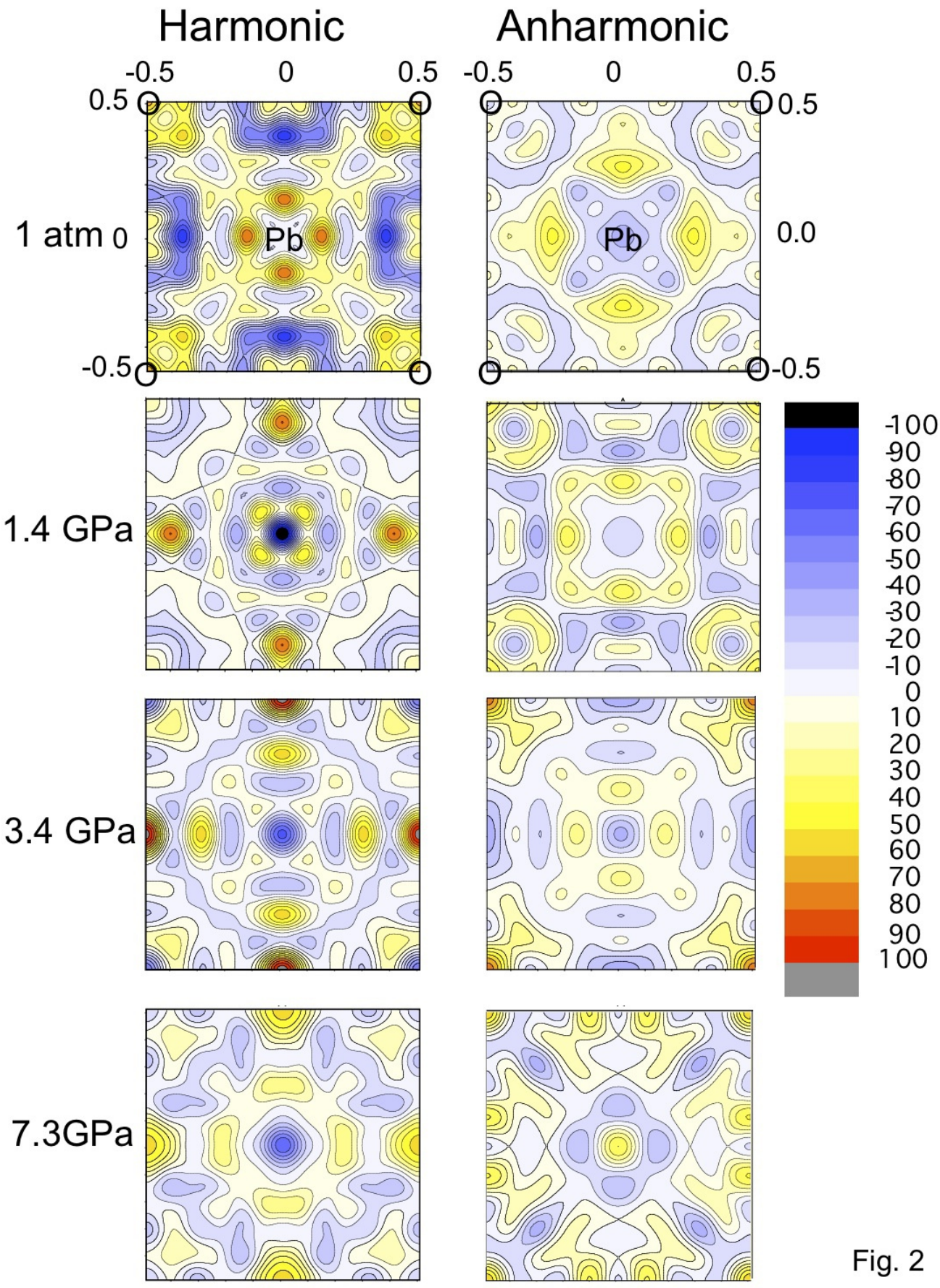
Harmonic
Anharmonic
-0.5
0
0.5
0.5
0
-0.5
1 atm
Pb
Pb
0.0
1.4 GPa
3.4 GPa
7.3GPa
-100
-90
-80
-70
-60
-50
-40
-30
-20
-10
0
10
20
30
40
50
60
70
80
90
100

Fig. 2

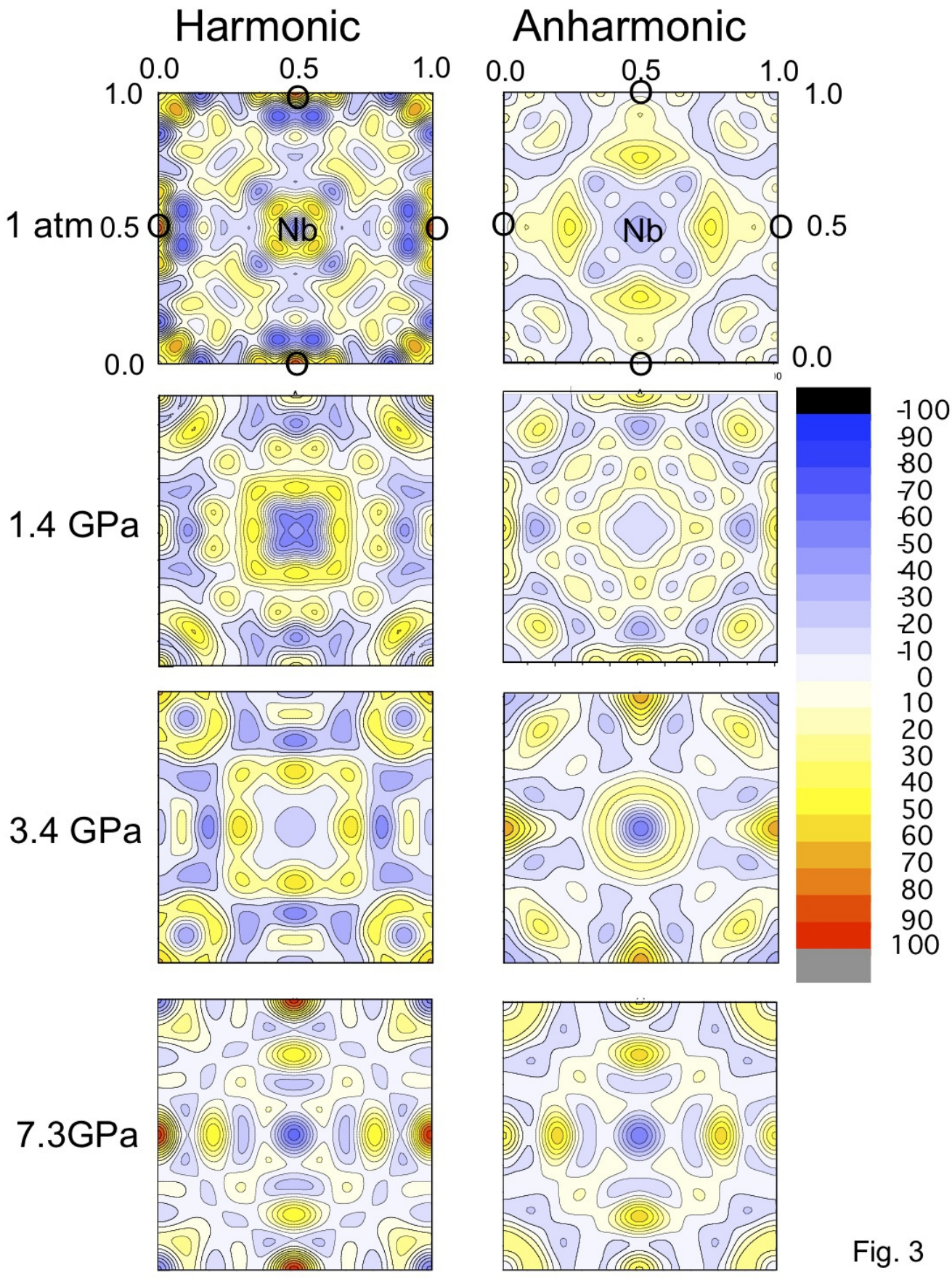
Harmonic
Anharmonic
0.0
0.5
1.0
1 atm
1.4 GPa
3.4 GPa
7.3GPa
Nb
O
-100
-90
-80
-70
-60
-50
-40
-30
-20
-10
0
10
20
30
40
50
60
70
80
90
100

Fig. 3

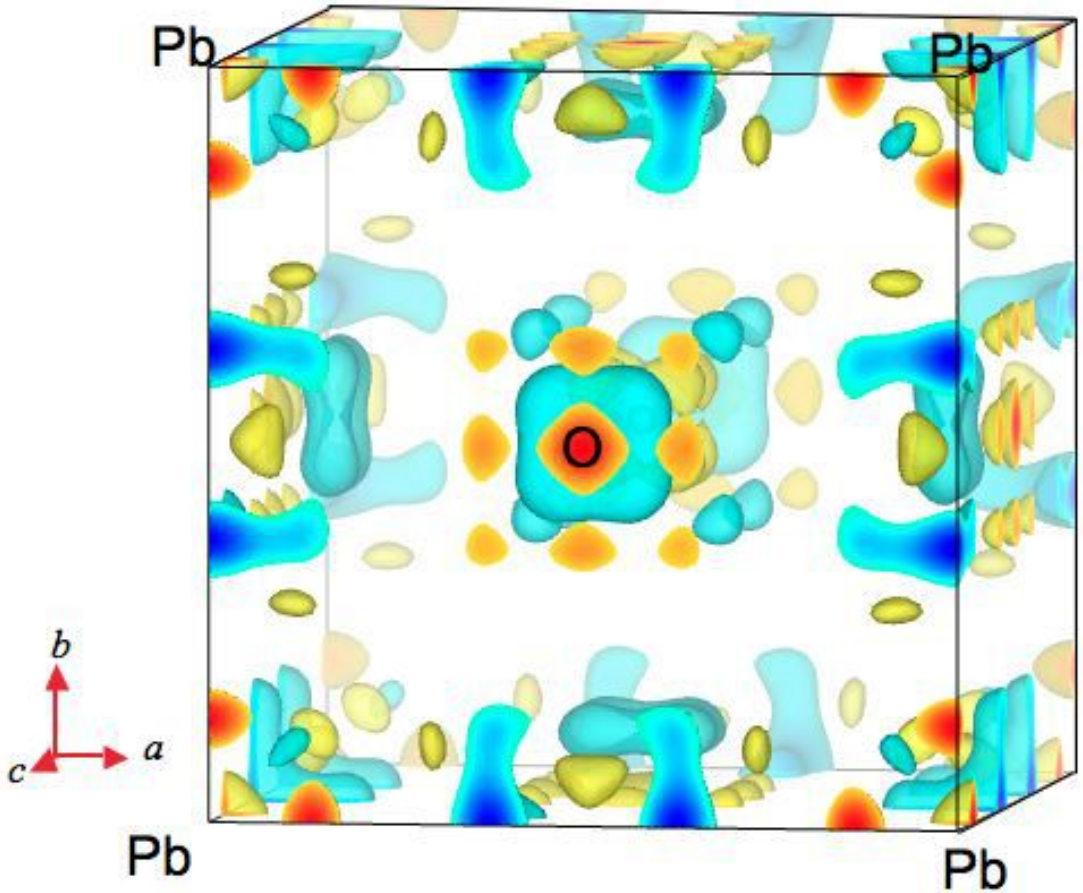

Fig. 4